Journal of Solid State Chemistry 181 (2008) 1833–1839

Contents lists available at ScienceDirect

Journal of Solid State Chemistry

journal homepage: www.elsevier.com/locate/jssc

Structural, magnetic and electronic properties of $LaNi_{0.5}Fe_{0.5}O_3$ in the temperature range 5–1000 K

M. Gateshki [a], L. Suescun [b,1], S. Kolesnik [c], J. Mais [c], K. Świerczek [b,c,2], S. Short [b], B. Dabrowski [b,c,*]

[a] Bragg Institute, Australian Nuclear Science and Technology Organization, Menai, NSW 2234, Australia
[b] Materials Science Division, Argonne National Laboratory, Argonne, IL 60439, USA
[c] Physics Department, Northern Illinois University, DeKalb, IL 60115, USA

ARTICLE INFO

Article history:
Received 27 December 2007
Received in revised form
21 March 2008
Accepted 31 March 2008
Available online 16 April 2008

Keywords:
Solid oxide fuel cells
Perovskites
Phase transitions

ABSTRACT

The structure, magnetism, transport and thermal expansion of the perovskite oxide $LaNi_{0.5}Fe_{0.5}O_3$ were studied over a wide range of temperatures. Neutron time-of-flight data have shown that this compound undergoes a first-order phase transition between ~275 and ~310 K. The structure transforms from orthorhombic (*Pbnm*) at low temperatures to rhombohedral ($R\bar{3}c$) above room temperature. This phase transition is the cause for the previously observed co-existence of phases at room temperature. The main structural modification associated with the phase transition is the change of tilting pattern of the octahedra from $a^+b^-b^-$ at low temperatures to $a^-a^-a^-$ at higher. Magnetic data strongly suggests that a spin-glass magnetic state exists in the sample below 83 K consistent with the absence of magnetic ordering peaks in the neutron data collected at 30 K. At high temperatures the sample behaves as a small polaron electronic conductor with two regions of slightly different activation energies of 0.07 and 0.05 eV above and below 553 K, respectively. The dilatometric data show an average thermal expansion coefficient of $14.7 \times 10^{-6}\,K^{-1}$ which makes this material compatible with frequently used electrolytes in solid oxide fuel cells.

1. Introduction

Materials with the chemical formula $LaNi_xFe_{1-x}O_3$ and perovskite structure have been extensively studied due to a wide range of electrical, magnetic, catalytic and other important properties [1–5]. For example, $LaNiO_3$ is a highly conducting (ρ~0.1 mΩ cm at 300 K, [6]) Pauli paramagnet with rhombohedral structure (space group $R\bar{3}c$, No. 167), while $LaFeO_3$ is an antiferromagnetic insulator (Neel temperature $T_N = 740$ K, [7]) with orthorhombic structure (space group *Pbnm*, No. 62). $LaNi_xFe_{1-x}O_3$ materials have shown very good catalytic properties for peroxide decomposition and oxygen reduction [8,9]. Recent research on cathode materials for solid oxide fuel cells (SOFC) indicate that $LaNi_xFe_{1-x}O_3$ and strontium substituted $La_{1-y}Sr_yNi_xFe_{1-x}O_3$ may satisfy several requirements for application at intermediate temperatures such as good chemical stability, high ionic and electronic conductivity, and low thermal expansion coefficient (TEC), which were studied with thermogravimetric analysis, resistivity, and dilatometry measurements [10–13].

Other experimental techniques used to study these materials include infrared spectroscopy [3]; Mössbauer spectroscopy [1,3,14,15]; magnetic measurements [1,9,14] and electrical resistivity measurements [2,16]. Despite this considerable interest, the structural properties of $LaNi_xFe_{1-x}O_3$ are not fully understood and have been a subject of some controversy in the literature. In [3] the structures of compositions $x = 0.1, 0.25, 0.5$ were reported as cubic, but no other details were given. More recent work [4] showed that the materials with $x = 0.1, 0.25, 0.4$ are orthorhombic and those with $x = 0.6, 0.75, 0.85, 0.9$ are rhombohedral. For the material with $x = 0.5$ both orthorhombic and rhombohedral phases were present in the sample. With respect to this last result it is interesting to mention that in [17] $LaNi_{0.5}Fe_{0.5}O_3$ was studied with high-pressure infrared spectroscopy (no structural studies were conducted) and the changes observed around 1.4 GPa were attributed to charge transfer between the Ni and Fe cations. So far, no detailed temperature-dependent structural studies of $LaNi_xFe_{1-x}O_3$ have been performed despite the observation of structural phase transitions in materials with similar compositions such as La_2CoMnO_6 and La_2NiMnO_6 [18]. We present here the results of structural and magnetic characterization of a stoichiometric $LaNi_{0.5}Fe_{0.5}O_3$ sample using neutron powder diffraction and magnetic measurements between 5 and 400 K.

* Corresponding author at: Materials Science Division, Argonne National Laboratory, Argonne, IL 60439, USA.
E-mail address: dabrowski@anl.gov (B. Dabrowski).
[1] Permanent address: Cryssmat-Lab/Detema, Facultad de Química, Universidad de la República, P.O. Box 1157, Montevideo, Uruguay.
[2] Permanent address: Faculty of Materials Science and Ceramics, AGH University of Science and Technology, al. Mickiewicza 30, 30-059 Krakow, Poland.

0022-4596/$ - see front matter © 2008 Elsevier Inc. All rights reserved.
doi:10.1016/j.jssc.2008.03.041

Together with complementary resistivity and dilatometry measurements over a temperature range 300–1073 K they clarify the structural behavior and allow to evaluate the properties of $LaNi_xFe_{1-x}O_3$ ($x = 0.5$) as SOFC cathode material.

2. Experimental

2.1. Synthesis and thermogravimetric measurements

A 6 g sample of $LaNi_{0.5}Fe_{0.5}O_3$ was prepared by solid-state reaction of pre-fired La_2O_3, Fe_2O_3 and NiO (all >99.99% purity, Alfa-Aesar). The starting 1:1/2:1 stoichiometric mixture of thoroughly ground oxides was pressed in a 13 mm pellet under 5 tons and first fired in air at 1173 K for 12 h. The material was then re-ground, pelletized and fired in air at 1623 K for several 12-h periods with intermediate re-grindings. X-ray diffraction data were collected after each firing using a Rigaku D-Max Powder Diffractometer to check the phase composition of the sample. After the second high-temperature firing the sample showed no change in the number or position of peaks but slight changes in the relative peak intensities were observed depending on the cooling rate applied to the sample. No traces of the original oxides or other intermediate products were detected in the patterns, which showed the presence of two slightly different phases. Stoichiometric oxygen content at 3.00 ± 0.01 was confirmed to 1073 K from thermogravimetric measurements in air and Ar (~20 ppm of O_2) followed by hydrogen reduction. At higher temperatures small amount of oxygen vacancies were observed, for example $\delta_{Ox} = 0.005$ and 0.03 at 1273 K in air and Ar, respectively.

Previous works [4,19] suggested the co-existence of rhombohedral and orthorhombic phases in $LaNi_{0.5}Fe_{0.5}O_3$ samples at room temperature (RT). An attempt was made to index the pattern with two phases yielding the expected mixture of orthorhombic ($a_o \approx \sqrt{2}a_p$, $b_o \approx \sqrt{2}a_p$, $c_o \approx 2a_p$) and rhombohedral ($a_r = b_r = c_r \approx \sqrt{2}a_p$, $\alpha = \beta = \gamma \approx 60^\circ$) phases ($a_p$ is the cubic simple perovskite lattice parameter). The two-phase behavior of the sample was later confirmed to be a consequence of a first-order structural phase transition close to RT, explaining the small changes in-phase ratio as a function of the cooling rate during preparation and the exact temperature of the data collection.

2.2. Physical properties measurements

The electrical resistivity was measured in air using the four-probe method with a home built apparatus between RT and 1273 K. Thermal expansion of the sample was measured using Linseis L75 dilatometer equipped with quartz holder and piston capable of performing measurements between RT and 1073 K. Two consecutive heating/cooling runs were performed in air with a temperature rate of 1°/min. TEC of the sample was evaluated from data obtained in the second cooling run, using correction for thermal expansion of quartz. Magnetic *ac* susceptibility and *dc* magnetization were measured by use of a Physical Property Measurement System Model 600 and a Magnetic Property Measurement System, respectively (both Quantum Design).

2.3. Neutron diffraction experiments and data analysis

Temperature-dependent neutron TOF diffraction data were collected at the Special Environment Powder Diffractometer (SEPD) at Argonne's Intense Pulsed Neutron Source [20]. This instrument is equipped with four detector banks located at 2θ angles of 144°, 90°, 44° and 22°. The first three banks cover considerable *Q*-range and are suitable for structural refinement. The fourth one is used for detection of diffraction peaks in the low-*Q*-range. The sample consisting of 5 g of $LaNi_{0.5}Fe_{0.5}O_3$ powder was placed in a vanadium can with a diameter of 1 cm, sealed in He and inserted into a Hot-stage Displex cryofurnace used for controlling the temperature. Seven different datasets were collected at 30, 100, 200, 250, 275, 300 and 400 K with 2 h of collection time for each temperature. Structural refinement and data correction were performed using the GSAS/EXPGUI suite of programs [21,22]. For all temperatures, the structural models were refined simultaneously against the diffraction data from the first three detector banks. This reduces the effect of possible calibration problems and allows obtaining structural data with very high quality. The experimental diffraction patterns collected at 30 K with three of the detector banks are shown in Fig. 1 together with

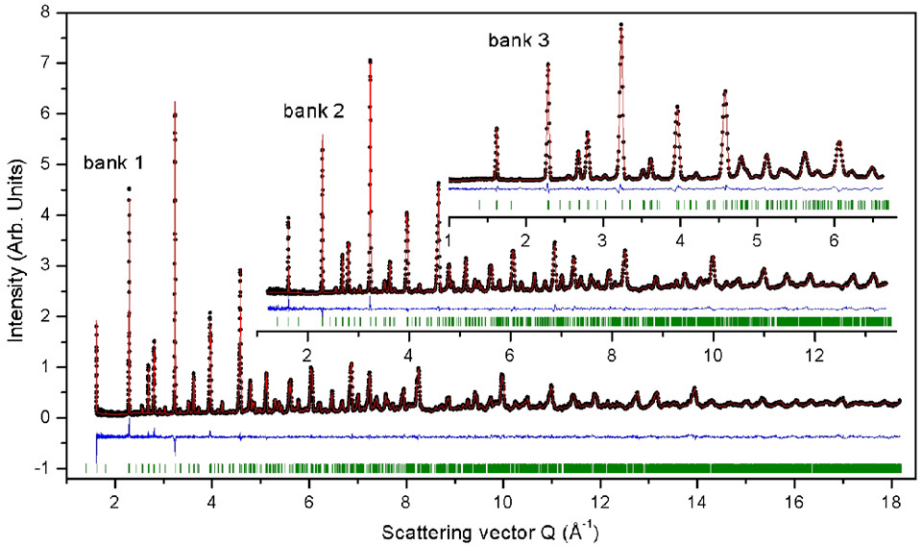

Fig. 1. Experimental diffraction profiles (symbols) of $LaNi_{0.5}Fe_{0.5}O_3$ collected at 30 K with the three detector banks (bank 1 at 144°; bank 2 at 90°; and bank 3 at 44°). The calculated and difference profiles (lines) are obtained after simultaneous Rietveld refinement of the crystal structure using the experimental profiles from the three banks. Vertical lines indicate the expected positions of structural peaks based on the *Pbnm* space group.

Table 1
Structural details of $LaNi_{0.5}Fe_{0.5}O_3$ obtained at different temperatures

SG	30 K	275 K		300 K		400 K
	Pbnm	Pbnm	$R\bar{3}c$	Pbnm	$R\bar{3}c$	$R\bar{3}c$
w. fr. %	100	90	10	21	79	100
a, Å	5.5087(1)	5.5181(1)	5.5175(3)	5.5182(4)	5.5199(1)	5.5222(1)
b, Å	5.4640(1)	5.4685(1)	5.5175(3)	5.4711(3)	5.5199(1)	5.5222(1)
c, Å	7.7439(1)	7.7509(1)	13.274(1)	7.7571(4)	13.2842(2)	13.3049(1)
La						
x	0.0037(2)	0.0030(3)	0	0.000(1)	0	0
y	0.0214(2)	0.0179(2)	0	0.016(1)	0	0
z	$\frac{1}{4}$	$\frac{1}{4}$	$\frac{1}{4}$	$\frac{1}{4}$	$\frac{1}{4}$	$\frac{1}{4}$
O1						
x	0.5644(2)	0.5638(4)	0.554(1)	0.568(2)	0.5546(2)	0.5542(1)
y	−0.0062(3)	−0.0049(4)	0	−0.010(2)	0	0
z	$\frac{1}{4}$	$\frac{1}{4}$	$\frac{1}{4}$	$\frac{1}{4}$	$\frac{1}{4}$	$\frac{1}{4}$
O2						
x	0.7731(2)	0.7700(2)	–	0.773(1)	–	–
y	0.2274(2)	0.2299(2)	–	0.227(8)	–	–
z	−0.0346(1)	−0.0339(1)	–	−0.033(1)	–	–
B_{La}, Å^2	0.25(1)	0.65(1)	–	–	0.52(1)	0.77(1)
B_M, Å^2	0.17(1)	0.31(1)	–	–	0.34(1)	0.40(1)
B_O, Å^2	0.44(1)	0.70(1)	–	–	0.84(1)	0.99(1)
χ^2	1.687	1.395		1.579		1.611

The atoms occupy the following Wyckoff positions: in *Pbnm*, La (4c: *x*,*y*, 1/4), M (4b: 1/2,0,0), O1 (4c: *x*,*y*, 1/4), O2 (8d: *x*,*y*,*z*); in $R\bar{3}c$, La (6a: 0,0,1/4), *M* (6b: 0,0,0), O (18e: *x*,0, 1/4). The data for the rhombohedral structure are given in hexagonal notation ($a = b$, $\gamma = 120^\circ$).
Note: Structural details at 100, 200 and 250 K are available as supplementary material.

the profiles calculated using the refined structural parameters given in Table 1.

3. Results and discussion

Fig. 2a shows the electrical conductivity of the sample presented in Arrhenius coordinates. A nonlinear characteristic may be observed with relatively high values of the order of 280 Scm^{-1} in the 873–1073 K range, with almost no temperature dependence in that range. These values are somewhat smaller than the ones measured for the best cathode materials based on Co, Fe, and Mn, but nevertheless still very attractive in terms of possible application of this material as a cathode in SOFC. Considering the fixed oxygen content of the sample below 1073 K the observed conductivity has to be considered as entirely electronic. For $LaNi_xFe_{1-x}O_3$ perovskites small polaron conduction mechanism was proposed [10]. The inset in Fig. 2a shows the electrical conductivity plotted in the $\log \sigma T$–$1/T$ coordinates. A linear dependence up to $T \approx 553$ K can be observed, suggesting small polaron mechanism of the electrical conductivity with activation energy equal to 0.05 eV. Above 553 K a little higher $E_a = 0.07$ eV was observed. The slight decrease of the electrical conductivity above 1073 K can be explained on the basis of formation of oxygen vacancies. It is expected that $LaNi_xFe_{1-x}O_3$ with $x > 0.5$ would exhibit higher electrical conductivity and form oxygen vacancies, which should lead to certain oxygen ion conductivity at elevated temperatures (>1073 K). A nonlinear dependence of the relative elongation of the sample was observed as a function of temperature in the RT–1073 K range (Fig. 2b) with much smaller elongation in temperatures close to RT. This phenomenon is probably a result of the structural phase transition which is discussed below. Similar disruptions in the linear behavior of relative elongation have been observed for $LaNi_xFe_{1-x}O_3$ ($x < 0.5$) samples at the transition temperatures between the low-temperature orthorhombic and high-temperature rhombohedral phases [12]. Calculated TEC is quite low (8.8×10^{-6} K^{-1}) in the temperature range RT–400 K. The elongation of the sample is much higher and TEC is equal to 16.8×10^{-6} K^{-1} for 573–1023 K range. The average expansion of the sample in the measured temperature range (14.7×10^{-6} K^{-1}) is similar to value observed for other $LaNi_xFe_{1-x}O_3$ perovskites and is similar to common electrolytes used in SOFC [10,12]. The expansion of $LaNi_{0.5}Fe_{0.5}O_3$ in the measured range should be considered as purely thermal as there is no chemical expansion due to increase of the ionic sizes of Fe and Ni caused by oxygen reduction.

Fig. 3 shows the temperature dependence of *dc* magnetization for $LaNi_{0.5}Fe_{0.5}O_3$, measured in a magnetic field of 1 kOe after cooling in a zero magnetic field (M_{ZFC}), on cooling in the same magnetic field (M_{FC}), and the remnant magnetization measured on warming after "field cooling" and switching off the magnetic field (M_{trm}). The *ac* susceptibility measured in the *ac* excitation field of 14 Oe at a frequency of 10 kHz is presented in the inset to Fig. 3. The observed cusp in the "zero field cooled" magnetization as well as the *ac* susceptibility is consistent with the presence of a spin-glass state in the sample below the freezing temperature $T_f = 80$ K. This behavior is supported by the observation of characteristic irreversibility between the "zero field cooled" and "field cooled" magnetizations and the presence of the remnant magnetization, which disappears on warming at the irreversibility temperature just below T_f. All these phenomena are fingerprints of the magnetic glassy behavior, usually present in frustrated magnetic systems with competing ferromagnetic and antiferromagnetic interactions.

The lack of observation of extra diffraction peaks or relative intensity changes in the 30 K dataset (Fig. 1) other than those expected from the nuclear structure is a clear indication of the absence of long-range magnetic ordering of Fe and Ni magnetic moments in the lattice in direct agreement with the magnetization data. This spin-glass behavior is expected to arise as a

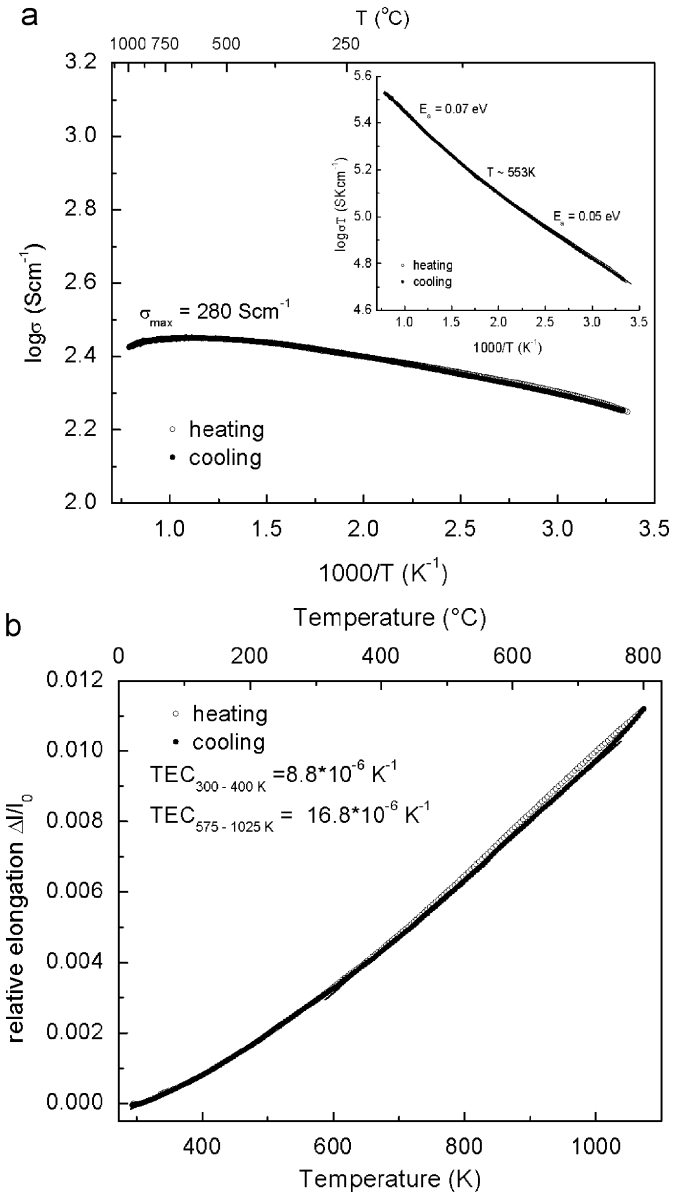

Fig. 2. (a) The electrical conductivity data for $LaNi_{0.5}Fe_{0.5}O_3$ sample collected between RT and 1273 K. The inset shows the data in the log σT–$1/T$ coordinates appropriate for the small polaron conduction mechanism. (b) The relative elongation of $LaNi_{0.5}Fe_{0.5}O_3$ sample collected between RT and 1073 K.

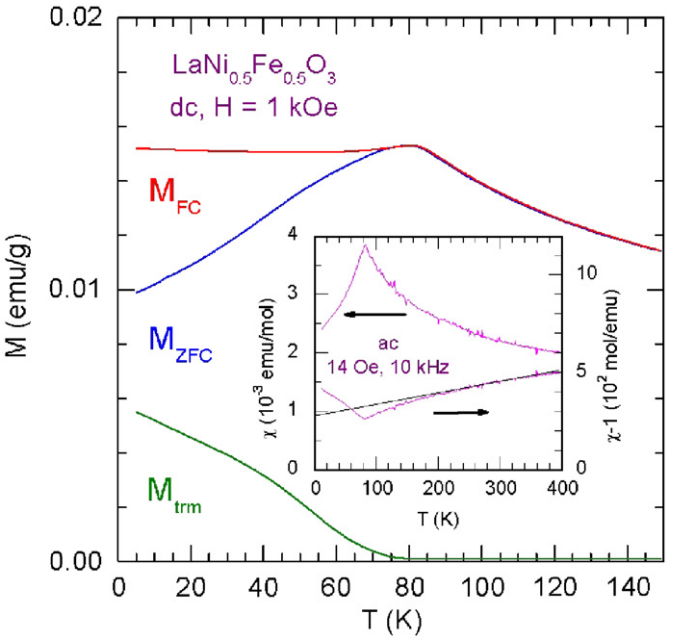

Fig. 3. Temperature dependence of *dc* magnetization for $LaNi_{0.5}Fe_{0.5}O_3$, measured in a magnetic field of 1 kOe after cooling in zero magnetic field (M_{ZFC}), on "field cooling" (M_{FC}), and remnant magnetization (M_{trm}). Inset: *ac* susceptibility measured in the *ac* excitation field of 14 Oe at a frequency of 10 kHz (left scale) and the inverse *ac* susceptibility (right scale). The straight line is a guide to the eye.

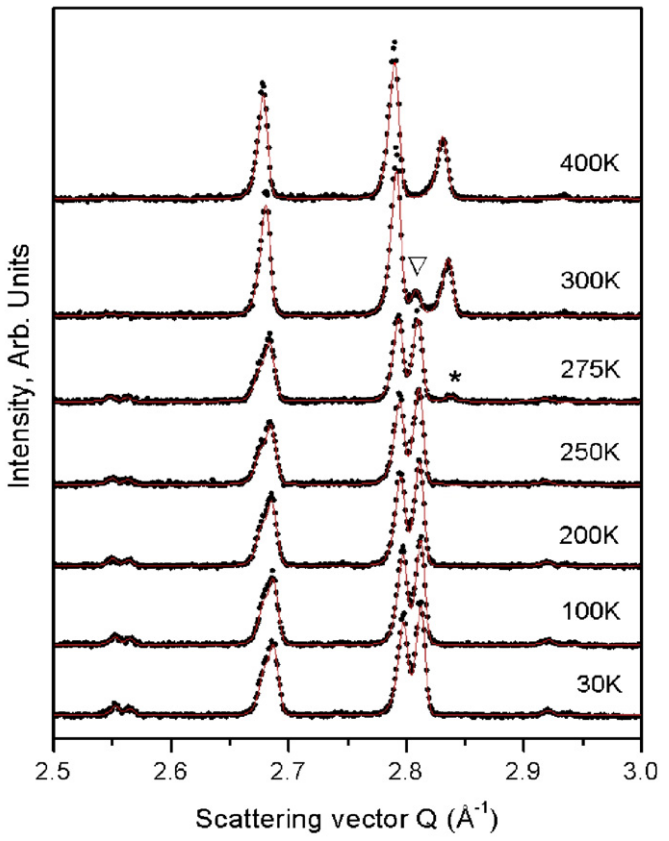

Fig. 4. Variation with temperature of the diffraction profile of $LaNi_{0.5}Fe_{0.5}O_3$. Between 30 and 250 K the experimental data (symbols) are well approximated by a single perovskite structure with orthorhombic symmetry. The emergence of the rhombohedral phase is observed at 275 K (peak marked with ×). At 300 K only a small amount of the orthorhombic phase remains (peak marked with ▽) and at 400 K only the rhombohedral phase is observed.

consequence of the different signs of the magnetic interactions among d^5 Fe^{3+}, d^4 Fe^{4+}, d^7 Ni^{3+} and d^8 Ni^{2+} present in the lattice according to the following equilibrium: $Fe^{3+}+Ni^{3+} \leftrightarrow Fe^{4+}+Ni^{2+}$. Application of the Goodenough–Kanamori rules to all the possible pairs of cations Fe–Fe, Fe–Ni and Ni–Ni yields that both ferromagnetic and antiferromagnetic interactions are expected in this B-site disordered perovskite generating the conditions for local ordering and eventual spin freezing at low temperatures. It has been previously suggested in [14] that a spin-glass behavior exists at low temperatures for $LaNi_xFe_{1-x}O_3$ ($x \geqslant 0.8$) appealing to multiplicity of interactions expected among the different magnetic centers found in the lattice. A plot of the inverse *ac* susceptibility as a function of temperature (inset to Fig. 3) shows that strong interactions among magnetic centers exist well above T_f The extrapolation of the slope of the curve for temperatures above T_f (the straight line in Fig. 3) always gives a negative intercept with the horizontal axis, which implies that the

prevalent interactions are antiferromagnetic below 400 K. The freezing temperature is unusually high (~80 K) which evidences the presence of strong local magnetic interactions in the sample, although the long-range magnetic order is absent.

From the diffraction profiles collected at temperatures between 30 and 250 K, portions of which are shown in Fig. 4, it was immediately established that $LaNi_{0.5}Fe_{0.5}O_3$ has orthorhombic perovskite structure similar to that observed in $LaFeO_3$ [23]. This structure has symmetry described by the space group *Pbnm* and presents octahedral tilting of the type $a^+b^-b^-$ according to the notation suggested by Glazer [24]. This tilting pattern involves in-phase rotations of the octahedra from two adjacent layers around one of the axes of the parent cubic perovskite structure and out-of-phase rotations with equal magnitudes around the other two axes. The presence of rock-salt ordering between the B-site cations is known [25,26] to give rise to diffraction reflections of the type $0\,k\,l$ ($k,l = 2n+1$). Such reflections however, were not observed in the patterns collected from $LaNi_{0.5}Fe_{0.5}O_3$, indicating that Ni and Fe atoms occupy the B-sites of the perovskite structure (centers of octahedra) with equal probability. The same result was obtained in [4] on the base of X-ray powder diffraction measurements. Interestingly, the related material La_2NiMnO_6 shows 85% of Ni:Mn ordering [18]. The diffraction pattern at 400 K is markedly different from those observed at low temperatures (see Fig. 4). On the other hand, this pattern is very similar to that observed in $LaNiO_3$ which has a rhombohedral perovskite structure with space group $R\bar{3}c$ and octahedral tilting $a^-a^-a^-$ (out-of-phase rotations with equal magnitudes around the three axes of the parent cubic structure). Refinement of the structure with this model converges rapidly and the calculated pattern approximates well the experimental one. Such structural transformation from *Pbnm* to $R\bar{3}c$ symmetry is observed for example in $LaCrO_3$ [27] and is required by group-theoretical considerations [28] to be of the first order. The diffraction profiles at 275 and 300 K show co-existence of both the orthorhombic and the rhombohedral phase in different proportions (see Table 1) which is consistent with the results in [4]. Such co-existence is typical for materials undergoing a first-order phase transition and is observed for example in $SrLaNiRuO_6$ [29] and Sr_2CoWO_6 [30]. On the other hand, the observation of a single perovskite phase at both low and high temperatures suggests that indeed this co-existence is due to the kinetics of the transition rather than to phase segregation related to compositional inhomogeneity of the material. The existence of a structural phase transition in $LaNi_{0.5}Fe_{0.5}O_3$ around RT is a very important fact and certainly must be included in the discussion of the charge-transfer effects observed previously around 1.4 GPa using high-pressure infrared spectroscopy [17].

Recent studies of structural phase transitions in perovskite materials [31,32] have shown that the temperatures at which phase transitions occur are determined by the composition of the materials and more specifically by the so-called tolerance factor $t = d_{A-O}/\sqrt{2}d_{B-O}$ which is a measure of the mismatch between the size of the A-site cation and the interstitial space between the BO_6 octahedra. This relation suggests that phase transitions similar to that observed in $LaNi_{0.5}Fe_{0.5}O_3$ around RT can be expected in the rest of the $LaNi_xFe_{1-x}O_3$ at different temperatures: lower than 300 K for the rhombohedral compounds ($x > 0.5$) and higher than 300 K for the orthorhombic ones ($x < 0.5$). This is confirmed by the observation of similar orthorhombic to rhombohedral phase transitions in $LaNi_{0.4}Fe_{0.6}O_3$ and $LaNi_{0.2}Fe_{0.8}O_3$ around 523 and 923 K, respectively [12].

The variation with temperature of the unit cell parameters and unit cell volume of $LaFe_{0.5}Ni_{0.5}O_3$ are shown in Fig. 5. It can be observed that there is a small discontinuity of the unit cell volume in the region where the phase transition occurs, however the general behavior shows a reduction of the volume at lower temperatures. The thermal expansion of the rhombohedral phase extracted from the variation of unit cell volume between 300 and 400 K was found to be $7.9 \times 10^{-6}\,K^{-1}$ which is consistent with the value of the TEC determined from dilatometry measurements in the same temperature range.

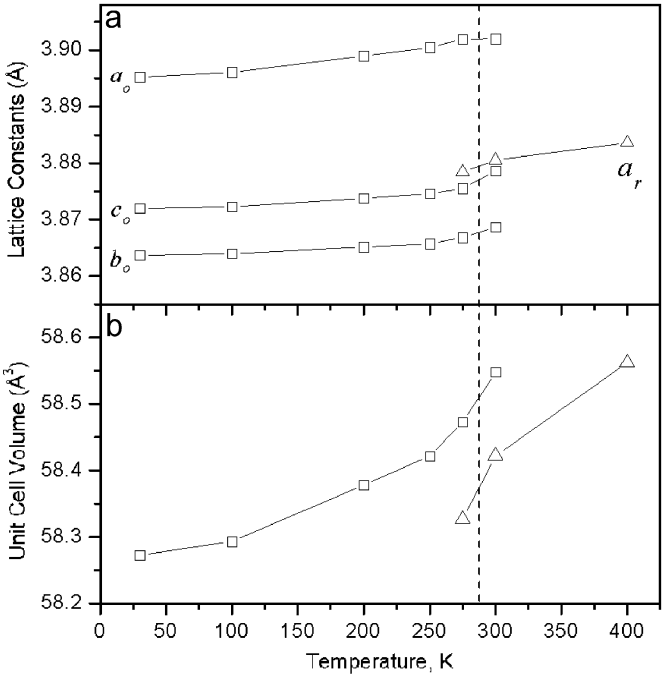

Fig. 5. Variation of lattice parameters (a) and unit cell volume (b) with temperature. For comparison, the values of lattice parameters for the orthorhombic (a_o, b_o, c_o) and rhombohedral phases (a_r) are referring to the simple perovskite unit cell.

To establish the microscopic mechanisms that lead to the volume decrease and shed light on the temperature-dependent structural changes occurring in perovskite materials we used the structural data given in Table 1 to calculate several representative microscopic parameters of the structure of $LaNi_{0.5}Fe_{0.5}O_3$.

The behavior of the average first-neighbor O–O, La–O and *M*–O (M = Ni,Fe) distances as a function of the temperature is shown in Fig. 6. It can be observed that when the structure changes from the rhombohedral to the orthorhombic phase there is a discontinuous increase in the average O–O and *M*–O distances which after that remain practically unchanged over the whole temperature range where the orthorhombic phase exists. It should be noted that the MO_6 octahedra are not perfectly regular; the three individual *M*–O distances have slightly different values and also that these individual distances change with temperature (see Fig. 6c). However, these changes proceed in such a manner that the average distance remain at a constant value. Based on bond-valence calculations [33] the expected Fe–O distances for a 6-coordinated Fe^{3+} cation in high spin configuration is 2.015 Å. Respectively, the expected Ni–O distance for a 6-coordinated Ni^{3+} cation in low spin configuration is 1.936 Å. The observed average *M*–O distance of 1.967 Å is close to the arithmetic mean of these expected values. Regarding the average La–O distance, after initial discontinuous increase across the phase transition it gradually decreases and at 30 K acquires a value similar to that at 400 K. These results are in very good agreement with the representation of the perovskite structure as a three-dimensional network of rigid octahedra, but help little in understanding the decrease of unit cell volume discussed above. Apart from the interatomic

distances, another important factor in the study of the distortion of the perovskite structures is the octahedral rotation or tilting. In the orthorhombic phase of $LaNi_{0.5}Fe_{0.5}O_3$, there are both in-phase (+) and out-of-phase (−) rotations. The rhombohedral phase has only out-of-phase rotations. The angles of the (+) and (−) rotations of the *Pbnm* structure were calculated using the following approximate formulae:

$$\varphi_o^{(-)} = \frac{1}{2}\left(\arctan\left[\frac{x(O1)-0.5}{0.25}\frac{\sqrt{2}a}{2c}\right] + \arctan\left[\frac{z(O2)}{\sqrt{\{(x(O2)-0.5)a\}^2+\{y(O2)b\}^2}}\frac{c}{a}\right]\right)$$

$$\varphi_o^{(+)} = \frac{1}{2}\left(\arctan\left[\frac{x(O2)-0.75}{0.25}\frac{a}{b}\right] + \arctan\left[\frac{0.25-y(O2)}{0.25}\frac{b}{a}\right]\right)$$

The calculation for $\varphi_o^{(+)}$is adapted from that suggested by Groen et al. [34] for ordered double perovskites. The calculation for $\varphi_o^{(-)}$ assumes that $y(O1)$ is negligible compared to $x(O1)$.

For the (−) rotation existing in the rhombohedral phase the formula used was

$$\varphi_r^{(-)} = \arctan\left[\frac{x(O)-0.5}{0.5}\right]$$

The angles calculated for the different temperatures are shown in Fig. 7. As seen, the angles of both (+) and (−) rotations of the orthorhombic phase increase at lower temperatures. The change of $\phi^{(-)}$ is about 0.1°, while that of $\phi^{(+)}$ is ~0.6°. From these results it can be concluded that the main contribution to the decrease of the unit cell volume at low temperatures comes from the increased in-phase rotation of the MO_6 octahedra.

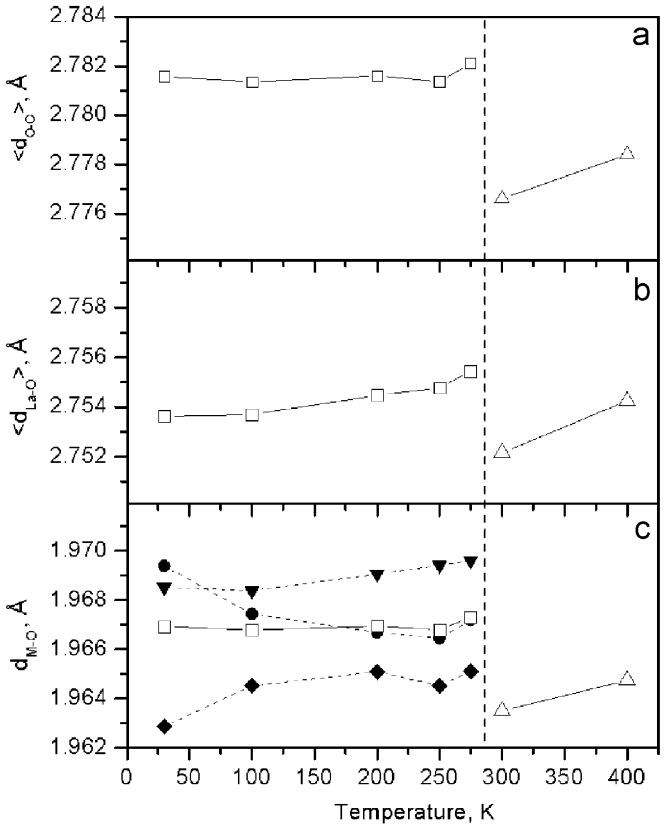

Fig. 6. Temperature dependence of the average first-neighbor O–O (a), La–O (b) and *M*–O (c) distances (open symbols) across the phase transition at ~300 K. In (c), the solid symbols represent the three individual *M*–O distances within the MO_6 octahedra.

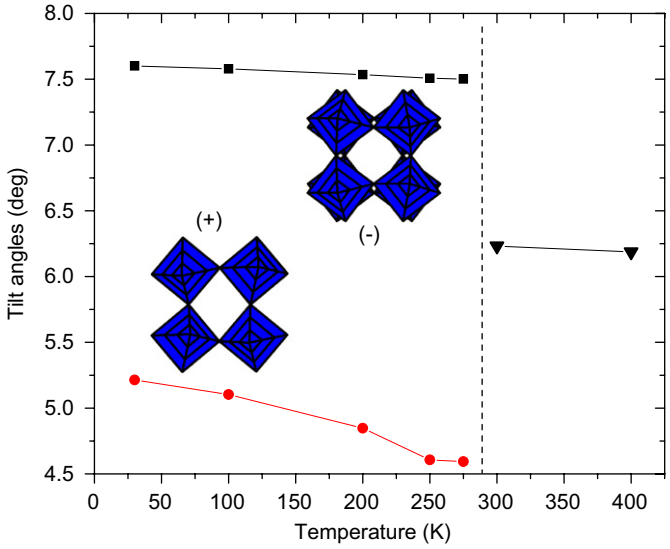

Fig. 7. Variation of the out-of-phase (black symbols) and in-phase (red symbols) octahedral rotations in $LaNi_{0.5}Fe_{0.5}O_3$.

4. Conclusions

From the point of view of application as a cathode material $LaNi_{0.5}Fe_{0.5}O_3$ may be an alternative to other cathode materials based on Fe, Co, and Mn only at temperatures higher than 1100 K as their electrical conductivity and thermal expansion coefficient are comparable. Unlike related compound $LaFeO_3$, $LaNi_{0.5}Fe_{0.5}O_3$ is paramagnetic above 83 K and shows spin-glass behavior below this temperature. This material has a perovskite structure with disordered arrangement of the Fe and Ni atoms over the B-sites. A first-order structural phase transition is observed close to RT during which the structure transforms from orthorhombic at lower temperatures to rhombohedral at higher. It is suggested that similar phase transitions may be present at higher temperatures for the other compounds of the $LaNi_xFe_{1-x}O_3$ ($x<0.5$) family. For $x>0.5$ the transition should move to lower temperatures and eventually disappear. In addition, the compositions with $x>0.5$ are expected to exhibit increased electrical and ionic conductivity. We have observed that the average *M*–O and O–O distances have constant values for the orthorhombic phase from 30 to 300 K. At the same time, the angle of in-phase octahedral rotations increases considerably and it was identified as the main microscopic mechanism for the reduction of the unit cell volume at low temperatures.

Acknowledgments

Work at NIU was supported by the NSF-DMR-0706610 and by the US Department of Transportation. Argonne National Laboratory's work was supported by the US Department of Energy, Office of Science, Office of Basic Energy Sciences, under contract DE-AC02-06CH11357.

Appendix A. Supplementary Materials

Supplementary data associated with this article can be found in the online version at doi:10.1016/j.jssc.2008.03.041.

References

[1] N.Y. Vasanthacharya, P. Ganguly, C.N.R. Rao, J. Solid State Chem. 53 (1984) 140–143.
[2] P. Ganguly, N.Y. Vasanthacharya, C.N.R. Rao, P.P. Edwards, J. Solid State Chem. 54 (1984) 400–406.
[3] P. Ganguly, N.Y. Vasanthacharya, J. Solid State Chem. 61 (1986) 164–170.
[4] H. Falcón, A.E. Goeta, G. Punte, R.E. Carbonio, J. Solid State Chem. 133 (1997) 379–385.
[5] S.M. de Lima, J.M. Assaf, Mater. Res. 5 (2002) 329–335.
[6] J.-S. Zhou, J.B. Goodenough, B. Dabrowski, Phys. Rev. Lett. 94 (2005) 226602.
[7] N.A. Halasa, G. DePasquali, H.G. Drickamer, Phys. Rev. B 10 (1974) 154–164.
[8] H. Falcón, R.E. Carbonio, J. Electroanal. Chem. 339 (1992) 69–83.
[9] R.E. Carbonio, C. Fierro, D. Tryk, D. Scherson, E. Yeager, J. Power Sources 22 (1988) 387–398.
[10] R. Chiba, F. Yoshimura, Y. Sakurai, Solid State Ion. 124 (1999) 281–288.
[11] R. Chiba, F. Yoshimura, Y. Sakurai, Solid State Ion. 152–153 (2002) 575–582.
[12] K. Świerczek, J. Marzec, D. Pałubiak, W. Zając, J. Molenda, Solid State Ion. 177 (2006) 1811–1817.
[13] K. Huang, H.Y. Lee, J.B. Goodenough, J. Electrochem. Soc. 145 (1998) 3220–3227.
[14] K. Asai, H. Sekizawa, J. Phys. Soc. Japan 49 (1980) 90–98.
[15] A.E. Goeta, G.F. Goya, R.C. Mercader, G. Punte, H. Falcón, R.E. Carbonio, Hyperfine Interact. 90 (1994) 371–375.
[16] A. Chainani, D.D. Sarma, I. Das, E.V. Sampathkumaran, J. Phys.: Condens. Matter 8 (1996) L631–L636.
[17] R. Mortimer, J.G. Powell, N.Y. Vasanthacharya, J. Phys.: Condens. Matter 9 (1997) 11209–11218.
[18] C.L. Bull, D. Gleeson, K.S. Night, J. Phys.: Condens. Matter 15 (2003) 4927–4936.
[19] N.V. Proskurnina, V.I. Voronin, V.A. Cherepanov, E.A. Kiselev, Progr. Solid State Chem. 35 (2007) 233–239.
[20] J.D. Jorgensen, J. Faber Jr.,, J.M. Carpenter, R.K. Crawford, J.R. Haumann, R.L. Hitterman, R. Kleb, G.E. Ostrowski, F.J. Rotella, T.G. Worlton, J. Appl. Cryst. 22 (1989) 321–333.
[21] A.C. Larson, R.B. Von Dreele, General structure analysis system (GSAS), Los Alamos National Laboratory Report LAUR 86–748, 2004.
[22] B.H. Toby, J. Appl. Cryst. 34 (2001) 210–213.
[23] M. Marezio, P.D. Dernier, Mater. Res. Bull. 6 (1971) 23–29.
[24] A.M. Glazer, Acta Crystallogr. B 28 (1972) 3384–3392.
[25] M. Gateshki, J.M. Igartua, Y. Brouard, Mater. Res. Bull. 38 (2003) 1661–1668.
[26] C.J. Howard, B.J. Kennedy, P.M. Woodward, Acta Crystallogr. B 59 (2003) 463–471.
[27] T. Hashimoto, N. Tsuzuki, A. Kishi, K. Takagi, K. Tsuda, M. Tanaka, K. Oikawa, T. Kamiyama, K. Yoshida, H. Tagawa, M. Dokiya, Solid State Ion. 132 (2000) 181–188.
[28] C.J. Howard, H.T. Stokes, Acta Crystallogr. B 54 (1998) 782–789.
[29] M. Gateshki, J.M. Igartua, Mater. Res. Bull. 38 (2003) 1893–1900.
[30] Q. Zhou, B.J. Kennedy, M.M. Elcombe, J. Solid State Chem. 180 (2007) 541–548.
[31] Q. Zhou, B.J. Kennedy, C.J. Howard, M.M. Elcombe, A.J. Studer, Chem. Mater. 17 (2005) 5357–5365.
[32] M. Gateshki, J.M. Igartua, A. Faik, J. Solid State Chem. 180 (2007) 2248–2255.
[33] N.E. Brese, M. O'Keeffe, Acta Crystallogr. B 47 (1991) 192–197.
[34] W.A. Groen, F.P.F. van Berkel, D.J.W. Ijdo, Acta Crystallogr. C42 (1986) 1472–1475.